ACS APPLIED MATERIALS & INTERFACES

Letter

www.acsami.org

Au-TiO_2 Nanoscale Heterodimers Synthesis from an Ambient Spark Discharge for Efficient Photocatalytic and Photothermal Activity

Jeong Hoon Byeon[†,*] and Young-Woo Kim[‡,*]

[†]Department of Chemistry, Purdue University, West Lafayette, Indiana 47907, United States

[‡]Department of Automotive Engineering, Hoseo University, Asan 336-795, Republic of Korea

Supporting Information

ABSTRACT: Ultrafine Au particles incorporating TiO_2 heterodimers were synthesized using an ambient heterogeneous spark discharge and the resultant materials were employed both in oxidizing photocatalytically CO gas and killing photothermally cancerous cells. Ti–Au spark configuration was employed to vaporize Ti and Au components into an airflow and finally ultrafine Au particles (~2 nm in lateral dimension) were incorporated with TiO_2 nanoparticles in the form of Au-TiO_2 heterodimers (~38 nm in lateral dimension) with enhanced photocatalytic (in CO oxidation) and photothermal activity (in cancerous cell killing) under visible light. We propose that the localized surface plasmon resonance of ultrafine Au particles on TiO_2 supports, induced by the visible light, would promote the adsorption-oxidation of CO and photothermal killing of HeLa cells. The present strategy may be suitable to fabricate other Au-metal oxide nanocomposites for catalytic and biomedical applications.

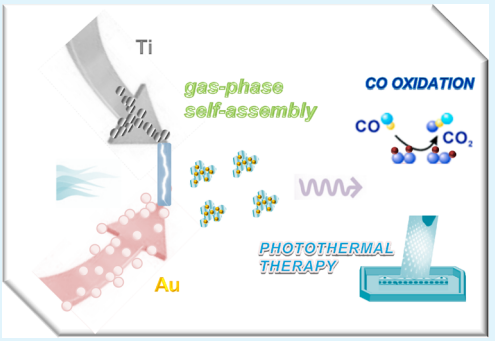

KEYWORDS: *Au-TiO_2, heterodimers, ambient heterogeneous spark discharge, CO oxidation, photothermal therapy*

INTRODUCTION

Nanoparticles are the building blocks for the fabrication of complex architectures because, on the one hand, they exhibit different physicochemical properties compared to the corresponding bulk material, and on the other hand, the interaction between them as a consequence of the spatial arrangement can have extraordinary properties that are not produced in the single-component.[1] Among them, metal oxide (e.g., TiO_2, ZnO, WO_3) nanoparticles have been frequently employed in environmental, energy, and display devices, as well as in biochemical sensors because of their unique band gap energy, anticorrosion property, physical sustainability, etc.[2]

However, the ability of pure TiO_2 in photocatalysis is currently required modifications to enhance their efficiency. One of the efficient modifications is to complex the metal oxides with noble metals such as Pd, Ag, and Au has been widely prepared and investigated. Particularly, Au has received much attention for its unique catalytic and optical properties.[3] Au nanoparticles could enhance the charge separation at the interfaces between Au and metal oxide because Au is well-known material as good electron sinks even for accumulating conditions.[4] The photocatalytic reactions of Au-TiO_2 heterodimers (complexation of nonidentical monomers) have been studied in hydrogen generation, site-selective metal deposition, solar cell fabrication, photosensors, and information devices.[5]

The present work introduces an ambient heterogeneous spark discharge to assemble Au-TiO_2 heterodimers for application to photocatalytic CO oxidation and photothermal cancerous cell killing. More recently, the Au-TiO_2 heterodimers have been extensively employed to enhance catalytic performance for catalytic CO conversion at low temperature conditions.[6] Another Au-TiO_2 heterodimer has been further employed to enhance photothermal killing of cancerous cells.[7] To the best of our knowledge, only a few studies have conducted the application of Au-TiO_2 heterodimers to biomedicine and catalysis, such as for anticancer modality, green energy, and environmental remediation applications.[7−9] Even though the heterodimers showed an enhancement in their specific applications, the multistep wet chemical steps with the use of toxic chemicals may not be suitable for their generalization.[10,11] On that account, a facile approach with greener processing is strongly required for the assembly or synthesis of hybrid nanostructures. In previous studies, we reported the creation of different carbonaceous/bimetallic nanostructures by controlling the conditions of heterogeneous spark discharges.[12,13] This is the first attempt to synthesize Au-TiO_2 heterodimers in a continuous gas-phase manner without using any wet chemical steps in an ambient environment. A Ti–Au spark configuration in an airflow environment was employed to produce Au-TiO_2 heterodimers, the heterodimers were collected using hydrophobic membrane filters, and finally they were detached before use both as photocatalysts to oxidize CO and as photosensitizers to kill cancerous cells (Scheme 1).

Received: November 7, 2013
Accepted: December 31, 2013
Published: December 31, 2013

Scheme 1. Ambient Heterogeneous Spark Discharge to Synthesize Au-TiO_2 Heterodimers in the Gas Phase for Photocatalytic and Photothermal Applications

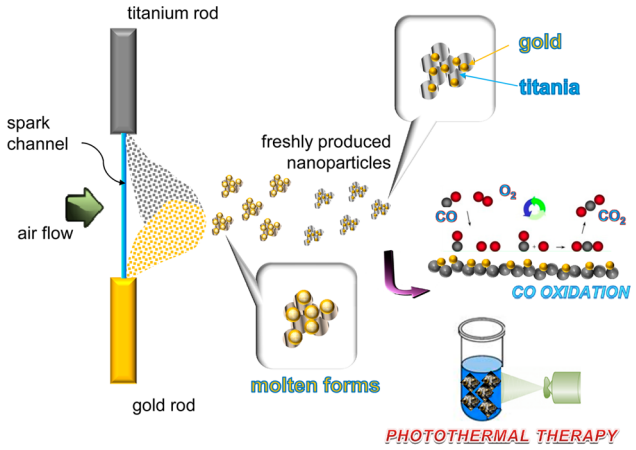

RESULTS AND DISCUSSION

A scanning mobility particle sizer (SMPS, 3936, TSI, US) was employed to measure the total number concentration (TNC), geometric mean diameter (GMD), and geometric standard deviation (GSD) of the Au particles, and the measured data were 1.87×10^7 particles cm^{-3}, 26.1 nm, 1.51, respectively, as shown in Figure 1. Au-TiO_2 heterodimers were formed near the

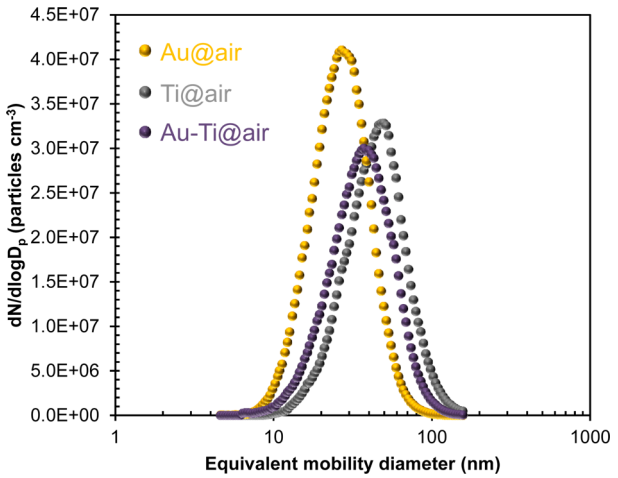

Figure 1. Size distributions of spark-produced individual Au and Ti particles their incorporated nanostructures (Au−Ti) under air flow environment. Standard deviations are described in Table 1

spark channel by incorporating Ti with Au under an existing O_2 environment. The incorporation of the TiO_2 particles with ultrafine Au particles was verified by gas-phase measurements of the size distributions for the different spark discharges. Table 1 shows the details of measurements of the Au, TiO_2, and Au-TiO_2 cases. The TNC, GMD, and GSD of the Au-TiO_2 case were 1.46×10^7 particles cm^{-3}, 35.3 nm, and 1.58, respectively. The analogous data for TiO_2 were 1.49×10^7 cm^{-3}, 43.3 nm, and 1.55, respectively. The size distribution of the Au-TiO_2 was between the Au and TiO_2 particles, and there were no additional peaks in the distribution, verifying that the nearly all Au was attached on the TiO_2, to form Au-TiO_2 heterodimers. In addition, the changes in size distribution through alternation of operation gas (N_2 to air) exhibited that there is a significant

Table 1. Details of the Size Distributions of Spark-Produced Individual Au and Ti Particles Their Incorporated Nanostructures (Au−Ti) under Air Flow Environment

case	GMD (nm)	GSD	TNC ($\times 10^7$ particles cm^{-3})
Au@air "Au"	26.1 ± 1.8	1.51	1.87
Ti@air "TiO_2"	43.3 ± 1.6	1.55	1.49
Au−Ti@air "Au-TiO_2"	35.3 ± 2.9	1.58	1.46

shift to larger sizes for the Au−Ti spark configuration (see Figure S1c in the Supporting Information) because of bindings between Ti and O atoms (see Figure S1a in the Supporting Information), whereas there is no size distribution shift in Au spark discharges (see Figure S1b in the Supporting Information).

Transmission electron microscope (TEM, JEM-3010, JEOL, Japan) images with low- and high-magnifications show the architecture of Au, TiO_2, and Au-TiO_2 samples. As shown in Figure 2, the TEM results confirm that both the Au (~24 nm in lateral dimension) and TiO_2 (~39 nm in lateral dimension) particles were agglomerates of primary particles, which is well agreement with the SMPS data noted in Table 1. As shown in the insets of Au and TiO_2, about 0.23 and 0.35 nm of the lattice fringes of Au and TiO_2 are observed, respectively, which can be respectively indexed as the (111) and (101) planes of the Au and TiO_2 structures. In addition, TEM measurements (see Figure S2 in the Supporting Information) showed that the resulting Au and Ti nanoparticles exhibited lattice fringes which were respectively consistent with the (111) and (100) diffraction planes of face-centered cubic Au (0.23 nm) and hexagonal close-packed Ti (0.26 nm),[14] in particular, the crystalline structure of Au was sustainable although the operation gas for their production was changed from N_2 to air. The Au-TiO_2 heterodimers essentially consisted of two kinds of particles. A darker contrast exhibits a diameter of ca. 2 nm and is assigned to Au nanoparticles, whereas a lighter-contrast one as a support, with a diameter of about 40 nm, is matched to the TiO_2 nanoparticles. This suggests that the heterogeneous spark discharge can be used to highly disperse Au particles on the surface of TiO_2. High-resolution TEM images show that the Au-TiO_2 heterodimers had both 0.23 [$Au_{(111)}$] and 0.35 [$TiO_{2(101)}$] nm in the lattice fringe.

A typical globular surface texture of the spark-produced Au-TiO_2 heterodimers following the morphology on a flat substrate was observed using a scanning probe microscope (SPM, IIIa, NanoScope, U.S.). The overlapped/protruded particles of bright contrast in Figure 3 may be identified with the presence of dispersed Au particles on TiO_2 supports, as is confirmed from the SPM. The ultrafine Au particles existed on TiO_2 supports could thus tightly attach on the TiO_2 surface, which may produce a strong metal−support interaction.

Figure 4a shows the CO conversion results of the Au-TiO_2 heterodimers using a photoirradiation device with a cutoff filter. With the introduction of visible light (>450 nm), the conversion of CO increased to about 47% at 20 °C. The conversion of CO decreased to about 29% when the visible light was turned off, but increased to about 36% again with reintroduction of the visible light (>600 nm). A better performance in photocatalysis than that of the pure TiO_2 nanoparticles (<4% in CO conversion at >450 nm irradiation) was attributed to the photoinduced electron−hole separation at the Au-TiO_2 interface that was facilitated by the close proximity

dx.doi.org/10.1021/am405004a | ACS Appl. Mater. Interfaces 2014, 6, 763−767

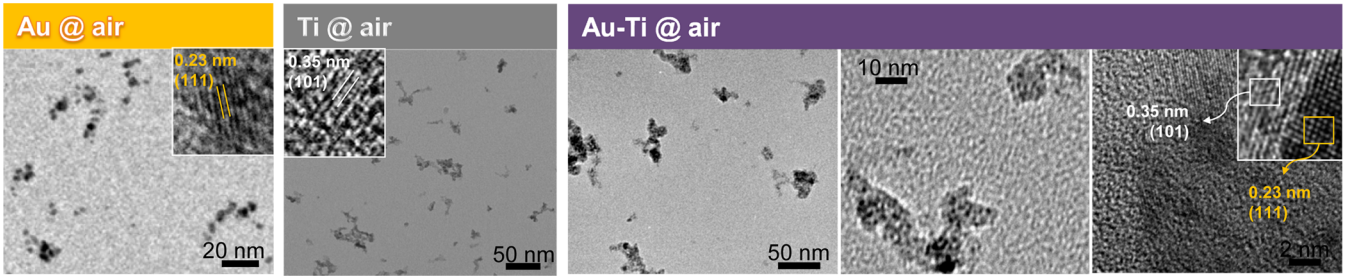

Figure 2. Low- and high-magnification TEM images of Au (24 ± 5.4 nm), TiO_2 (39 ± 7.6 nm), and Au-TiO_2 (38 ± 10.1 nm) samples.

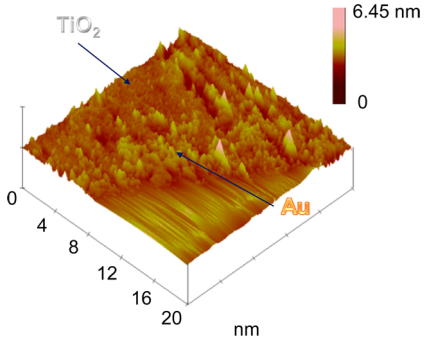

Figure 3. 3D topograph image of Au-TiO_2 heterodimers.

of the ultrafine Au particles. The adsorbed O_2 molecules on the surface of the heterodimers can trap the photoinduced electrons to generate the radicals for CO conversion. On the other hand, it is found that the >600 nm irradiation did not significantly promote the conversion of CO, which implies that the TiO_2 support cannot catalytically oxidize CO under visible light irradiation. N_2 adsorption measurements (via a Micromeritics ASAP 2010 apparatus) were employed to determine the textural property of the Au-TiO_2 heterodimers and to verify the production of interconnected pores in the heterodimers (inset of Figure 4a). The measured isotherm of the Au-TiO_2 heterodimers indicates its meso- and macro-porous characteristics. The uptakes at >0.85 and <0.85 of $P\ P_0^{-1}$ may originate from the void spaces between agglomerated Au-TiO_2 and between Au and TiO_2, respectively.[15] The pores within Au-TiO_2 heterodimers could show an appropriate structure for adsorbing CO, which eventually led to enhanced photocatalytic performances in CO oxidation. Figure 4b shows Fourier transform infrared spectra (IFS 66/S, Bruker Optics, Germany) of Au-TiO_2 samples before and after CO oxidation. As compared to the spectrum of Au-TiO_2 without adsorbing CO, a feature at ~2180 cm^{-1}, with another shoulder at ~2160 cm^{-1}, that appeared on the sample was caused by CO adsorption on Au-TiO_2. CO adsorbed on Au-TiO_2 heterodimers is consumed by reaction with O_2 at the interface. Moreover, a shifted peak at a lower frequency (~2080 cm^{-1}) was also introduced because of another correspondence of the CO adsorption with photocatalysis.[16] The IR spectrum also shows the existence of TiO_2 particles, other bands at around 850 cm^{-1} assigned to Ti−O and TiO_2 stretching,[17] verifying that TiO_2 nanocrystals exist within the heterodimers. This incorporation may be of value to transfer carriers and induce a synergistic effect to enhance the photocatalytic activity.

We further tested the efficiency of the heterodimers to transfect HeLa cells using plasmid DNA (pDNA) that contain the luciferase and EGFP gene. In order to give positive surface polarity of the Au-TiO_2 heterodimers (inset of Figure 5a), poly

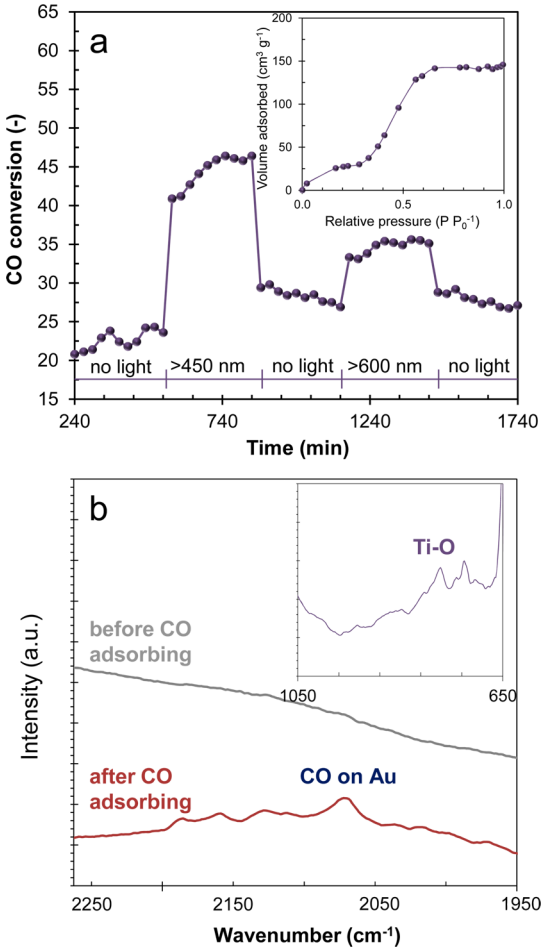

Figure 4. Photocatalytic performances of Au-TiO_2 heterodimers in CO oxidation. (a) Photocatalytic responses of Au-TiO_2 heterodimers with different wavelength ranges (>450 and >600 nm with on−off). Adsorption isotherm of Au-TiO_2 heterodimers is also shown as the inset. (b) IR spectra of adsorbing CO over Au-TiO_2 heterodimers under different conditions: before adsorbing CO and after adsorbing CO under visible light (>450 nm) irradiation. Another IR spectrum at the different frequency range to verify existence of TiO_2 is also displayed as the inset.

L-lysine (PLL) was directly incorporated on the heterodimers through Byeon−Roberts method.[18] Zeta potential of Au-TiO_2@PLL nanocomposites was ~14 mV by controlling PLL concentration. The transfection efficiency of nanocomposites-pDNA complexes in the cell line was greater than that of individual pDNA (Figure 5a). The ability for the nanocomposites was the greatest, even greater than those of polyethyelenimine (PEI) and chitosan. Another inset in Figure

dx.doi.org/10.1021/am405004a | ACS Appl. Mater. Interfaces 2014, 6, 763−767

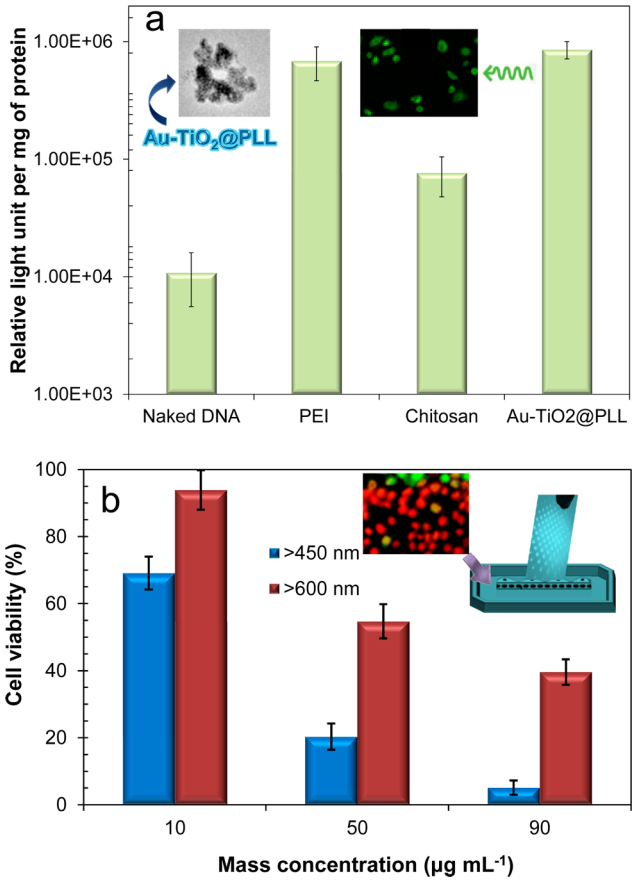

Figure 5. In vitro measurements of Au-TiO_2 heterodimers in gene transfection efficiency and photothermal cell killing. (a) Gene transfection efficiency of Au-TiO_2@PLL nanocomposties (inset TEM image) including naked DNA, PEI, and chitosan reference samples. A fluorescent microscope image for Au-TiO_2@PLL-EGFP complexes is also displayed as another inset. (b) Cell viability with different wavelength ranges (>450 and >600 nm) for Au-TiO_2@PLL nanocomposites with different mass concentrations ranged 10−90 μg mL^{-1}. A representative fluorescent image after the irradiation is also displayed as the inset.

5a shows the fluorescent microscope image of the HeLa cells for the nanocomposites induced by EGFP, which also verified their transfection. The greater efficiency of the Au-TiO_2@PLL nanocomposites may have originated from the incorporation of high affinity between the luciferase and composites and smaller size (~53 nm) of the nanocomposites (cf. ~120 nm for PEI and ~165 nm for chitosan). In order to investigate the potential of the synthesized nanocomposites as photosensitizers, suspensions of the nanocomposites in agar were irradiated with the different lights (>450 nm and >600 nm) emitted by a photoirradiation system with a cutoff filter (Scheme 1). This wavelength was chosen since it was relatively close to the peak value of the Au-TiO_2 heterodimers determined by UV−vis spectroscopy (see Figure S3a in the Supporting Information). The agar phantom was used to mimic physiological conditions. To briefly confirm the feasibility of the nanocomposites in photothermal therapy, we further employed adenosine triphosphate (ATP) assay. In a previous report, it is proved that viability of most cancer cells strongly related to their glycolysis for ATP production.[19] In the presence of the nanocomposites in the cell lines, the light radiation inhibited ATP generation (which can also be verified using a fluorescence microscope, as shown in the inset of Figure 5b), whereas in the absence of the nanocomposites, the radiation did not affect the inhibition of ATP production. It may be suggested that the light energy delivered to the cell promotes the nanocomposites to an electronically excited state from which a number of reactive radical species ($^{\bullet}OH$, H_2O_2, and $O_2^{\bullet-}$)[7,20] and heats are generated via electron and energy transfer processes.[21] The cell viability using Au-TiO_2 heterodimers revealed the combination of photoinduced radical and heat generation. As a result, irreversible thermochemical modifications of a variety of cell constituents are induced.

From the discussion above, it is suggested that Au incorporation on TiO_2 through ambient heterogeneous spark discharge is not only an effective way to enhance photocatalytic activity but also a promising method to obtain photothermal killing of cancerous cells.

CONCLUSIONS

This work introduced for the first time an ambient plasma synthesis of Au-TiO_2 nanoscale heterodimers through an ambient heterogeneous spark discharge without any wet chemical preparations, and we further examined their photocatalytic and photothermal performances. The gas-phase incorporation of Au and TiO_2 did enhance contact between the Au and TiO_2 and facilitate efficient functions for photocatalytic and photothermal activities both in CO oxidation and photothermal cell killing. We believe this provides new perspectives and useful information for low-cost and more efficient photocatalysts and photosensitizers for environmental remediation and biomedical applications.

ASSOCIATED CONTENT

Supporting Information

The experimental procedure and size distributions and TEM images of Au, Ti and Au−Ti nanoparticles under N_2 gas flow environment. UV−vis spectra of Au, TiO_2, and Au-TiO_2 samples, and XRD and XPS spectra of the Au-TiO_2 heterodimers. This material is available free of charge via the Internet at http://pubs.acs.org/.

AUTHOR INFORMATION

Corresponding Authors

*E-mail: jbyeon@purdue.edu. Tel.: +1-765-494-5499.
*E-mail: ywkim@hoseo.edu. Tel.: +82 41 540 5819. Fax: +82 41 540 5818.

Notes

The authors declare no competing financial interest.

REFERENCES

(1) Heiligtag, F. J.; Rossell, M. D.; Süess, M. J.; Niederberger, M. *J. Mater. Chem.* **2011**, *21*, 16893−16899.
(2) Pradhan, S.; Ghosh, D.; Chen, S. *ACS Appl. Mater. Interfaces* **2009**, *1*, 2060−2065.
(3) Wang, H.; Faria, J. L.; Dong, S.; Chang, Y. *Mater. Sci. Eng., B* **2012**, *177*, 913−919.
(4) Awate, S. V.; Deshpande, S. S.; Rakesh, K.; Dhanasekaran, P.; Gupta, N. M. *Phys. Chem. Chem. Phys.* **2011**, *13*, 11329−11339.
(5) Ke, X.; Zhang, X.; Zhao, J.; Sarina, S.; Barry, J.; Zhu, H. *Green Chem.* **2013**, *15*, 236−244.
(6) Green, I. X.; Tang, W.; Neurock, M.; Yates, J. T., Jr. *Science* **2011**, *333*, 736−739.
(7) Abdulla-Al-Mamun, M.; Kusumoto, Y.; Zannat, T.; Islam, M. S. *Phys. Chem. Chem. Phys.* **2011**, *13*, 21026−21034.

(8) Fang, J.; Cao, S.-W.; Wang, Z.; Shahjamali, M. M.; Loo, S. C. J.; Barber, J.; Xue, C. *Int. J. Hydrogen Energy* **2012**, *37*, 17853−17861.
(9) Yang, Y.-F.; Sangeetha, P.; Chen, Y.-W. *Int. J. Hydrogen Energy* **2009**, *34*, 8912−8920.
(10) Belova, V.; Borodina, T.; Möhwald, H.; Shchukin, D. G. *Ultrason. Sonochem.* **2011**, *18*, 310−317.
(11) Zhang, J.; Liu, X.; Wang, S.; Wu, S.; Cao, B.; Zheng, S. *Powder Technol.* **2012**, *217*, 585−590.
(12) Byeon, J. H.; Kim, J.-W. *Appl. Phys. Lett.* **2010**, *96*, 153102.
(13) Byeon, J. H.; Park, J. H.; Hwang, J. *J. Aerosol Sci.* **2008**, *39*, 888−896.
(14) Corrias, A.; Mountjoy, G.; Gozzi, D.; Latini, A. *Nanotechnology* **2007**, *18*, 485610.
(15) Jia, R.; Chen, J.; Zhao, J.; Zheng, J.; Song, C.; Li, L.; Zhu, Z. *J. Mater. Chem.* **2010**, *20*, 10829−10834.
(16) Liu, J.; Si, R.; Zheng, H.; Geng, Q.; Dai, W.; Chen, X.; Fu, X. *Catal. Commun.* **2012**, *26*, 136−139.
(17) Fan, W.; Lai, Q.; Zhang, Q.; Wang, Y. *J. Phys. Chem. C* **2011**, *115*, 10694−10701.
(18) Byeon, J. H.; Roberts, J. T. *ACS Appl. Mater. Interfaces* **2012**, *4*, 2693−2698.
(19) Huang, H.; Liu, N.; Guo, H.; Liao, S.; Li, X.; Yang, C.; Liu, S.; Song, W.; Liu, C.; Guan, L.; Li, B.; Xu, L.; Zhang, C.; Wang, X.; Dou, Q. P.; Liu, J. *PLoS One* **2012**, *7*, e49062.
(20) Abdulla-Al-Mamun, M.; Kusumoto, Y.; Zannat, T.; Islam, M. S. *Appl. Catal. A* **2011**, *398*, 134−142.
(21) Zedan, A. F.; Moussa, S.; Terner, J.; Atkinson, G.; El-Shall, M. S. *ACS Nano* **2013**, *7*, 627−636.